ADIPOCYTE
2025, VOL. 14, NO. 1, 2494089
https://doi.org/10.1080/21623945.2025.2494089

Taylor & Francis
Taylor & Francis Group

Atoh8 expression inhibition promoted osteogenic differentiation of ADSCs and inhibited cell proliferation in vitro and rat bone defect models

Zian Yi[a], Shuang Song[b], Yuxin Bai[c], Guanhua Zhang[d], Yuxi Wang[c], Zijun Chen[c], Xuefeng Chen[e], Banglian Deng[e], Xiangdong Liu[f], and Zuolin Jin[a]

[a]State Key Laboratory of Oral & Maxillofacial Reconstruction and Regeneration & National Clinical Research Center for Oral Diseases & Shaanxi Clinical Research Center for Oral Diseases, Department of Orthodontics, School of Stomatology, Air Force Medical University, Xi'an, China; [b]Key Laboratory of Shaanxi Province for Craniofacial Precision Medicine Research, College of Stomatology, Xi'an Jiaotong University, Xi'an, China; [c]State Key Laboratory of Oral & Maxillofacial Reconstruction and Regeneration & National Clinical Research Center for Oral Diseases & Shaanxi Clinical Research Center for Oral Diseases, Department of Oral Implantology, School of Stomatology, Air Force Medical University, Xi'an, China; [d]Department of Stomatology, Electric Power Teaching Hospital, Capital Medical University, Beijing, China; [e]Lianbang Research Institute of Oral Technology, Lianbang Hospital of Stomatology, Xi'an, China; [f]State Key Laboratory of Oral & Maxillofacial Reconstruction and Regeneration & National Clinical Research Center for Oral Diseases & Shaanxi Clinical Research Center for Oral Diseases, Department of Trauma and Orthognathic Surgery, School of Stomatology, Air Force Medical University, Xi'an, China

ABSTRACT

Stem cell-based bone tissue engineering offers a promising approach for treating oral and craniomaxillofacial bone defects. This study investigated the role of Atoh8, a key regulator in various cells, in the osteogenic potential of adipose-derived stem cells (ADSCs). ADSCs transfected with small interfering RNA (siRNA) targeting Atoh8 were evaluated for proliferation, migration, adhesion, and osteogenic capacity. In vivo, 20 SD rats were used to assess bone regeneration using Atoh8-knockdown ADSC sheets, with new bone formation quantified via micro-CT and histological analysis. Atoh8 knockdown in vitro reduced ADSC proliferation and migration but enhanced osteogenic differentiation and upregulation of osteogenic-related factors. This approach improved bone healing in rat defect models, accelerating repair both in vitro and in vivo. The findings underscore the clinical potential of ADSCs in bone tissue engineering and elucidate Atoh8's regulatory role in ADSC osteogenesis, providing a novel therapeutic strategy for enhancing bone regeneration through targeted modulation of stem cell differentiation pathways.

ARTICLE HISTORY
Received 30 October 2024
Revised 2 April 2025
Accepted 10 April 2025

KEYWORDS
Atoh8; adipose-derived stem cells; osteogenic differentiation; bone repair; stem cell transplantation

Introduction

Pathological factors such as trauma, inflammation, and tumours often cause bone defects of varying degrees, making bone defects one of the clinically challenging issues to resolve. Bone defects and related diseases can impair patients' functionality, leading to varying degrees of disability, and adversely affecting their quality of life and mental health [1,2].

Bone tissue engineering has demonstrated significant advantages in the treatment of clinical bone defects and has garnered widespread attention from scholars both domestically and internationally in recent years. With the rapid development of bone tissue engineering, adult stem cells have been proven to accelerate bone repair and improve prognosis [3]. The integration of bone tissue engineering, stem cell technology, and modern surgical techniques has opened new possibilities for the treatment of bone defects [4,5]. Mesenchymal stem cells (MSCs) are progenitor cells of various tissue cells, possessing remarkable multidirectional differentiation potential and self-renewal capabilities. They can migrate to injured sites and differentiate into local components of the injured area while secreting chemokines, cytokines, and growth factors that aid in tissue regeneration, playing a crucial role in regenerative medicine [6,7]. Among them, bone marrow mesenchymal stem cells (BMSCs) are the most widely used in clinical tissue repair due to their direct derivation from bone marrow. However, the content of MSCs in bone marrow is extremely low, accounting for less than 0.01% of the total number of monocytes [8]. Furthermore, the collection of BMSCs is accompanied by issues such as patient pain and significant trauma in clinical applications

CONTACT Xiangdong Liu liuxiangdong@fmmu.edu.cn State Key Laboratory of Oral & Maxillofacial Reconstruction and Regeneration & National Clinical Research Center for Oral Diseases & Shaanxi Clinical Research Center for Oral Diseases, Department of Trauma and Orthognathic Surgery, School of Stomatology, Air Force Medical University, No. 145, Changle West Road, Xincheng District, Xi'an, Shaanxi 710032, China; Zuolin Jin zuolinj@163.com State Key Laboratory of Oral & Maxillofacial Reconstruction and Regeneration & National Clinical Research Center for Oral Diseases & Shaanxi Clinical Research Center for Oral Diseases, Department of Orthodontics, School of Stomatology, Air Force Medical University, No. 145, Changle West Road, Xincheng District, Xi'an, Shaanxi 710032, China

[9]. Surprisingly, human adipose tissue is ubiquitous and can be easily and abundantly obtained through minimally invasive techniques. Patricia A. Zuk et al. [10] obtained human adipose tissue through liposuction, processed it to obtain a fibroblast-like stem cell population, and verified its multidirectional differentiation potential. Compared to BMSCs, adipose-derived stem cells (ADSCs) possess unique advantages such as abundant sources, easy access, minimal trauma, and strong immunomodulatory capabilities. Nevertheless, despite these advantages, the application of ADSCs in bone tissue engineering faces challenges. The osteogenic potential of ADSCs is generally lower than that of BMSCs, which may necessitate overcoming through genetic engineering or optimizing culture conditions.

Atoh8 belongs to the bHLH transcription factor family and it is a member of the 'Net' family within the 'Atonal' superfamily [11]. Atoh8 has been discovered to regulate cell fate and differentiation, particularly during development. It is expressed in the developing nervous system, where it modulates the differentiation of neurons and glial cells, determining the fate of neuronal precursor cells and potentially regulating the function of mature neurons [12]. Experiments conducted on C2C12 mouse myoblasts suggest that Atoh8 could play a regulatory role in the transition of myoblasts from a proliferative state to differentiation [13]. Interestingly, Atoh8 participates in stem cell growth and differentiation. Long non-coding RNA CIR inhibits the expression of Atoh8 through EZH2-mediated epigenetic modifications, thereby suppressing chondrogenic differentiation of human umbilical cord mesenchymal stem cells. The knockdown of CIR or the overexpression of Atoh8 promotes chondrogenic differentiation [14]. Another study in mice also indicates that Atoh8 is a critical regulator of neuronal differentiation during retinal development, and its absence inhibits the differentiation of retinal stem cells [15]. Additionally, some scholars have found that Atoh8 plays a pivotal role in tumour progression and stem cell transformation by regulating metabolism and cell fate decisions under stress conditions [16]. These studies highlight the important regulatory effects of Atoh8 in stem cell differentiation. However, it is still unknown whether Atoh8 affects the osteogenic differentiation of stem cells. Yahiro Y, et al. have found that Atoh8-KO primary osteoblasts and ST-2 cells with Atoh8 knockdown via transfection of Atoh8 small interfering RNA (siRNA) enhanced the osteogenic differentiation in in vitro experiments, with the increased expression of such osteogenic-specific genes as RUNX2 and ALP [17]. Based on these findings, we hypothesized that Atoh8 could negatively regulate the osteogenic differentiation of ADSCs. To verify this hypothesis, we conducted both in vitro and in vivo experiments to explore the regulatory effects of Atoh8 in ADSCs osteogenesis.

Material and methods

Extraction, cultivation, and differentiation induction of ADSCs

All animal procedures were conducted in accordance with the guidelines of the Chinese Council on Animal Protection and Use. All experiments in this study were approved by the Animal Protection and Ethics Committee of Air Force Medical University(Appl. No. kq-2024–033). The SD rats used were purchased from the Animal Experiment Center of Air Force Medical University and housed in an environmentally controlled room (20–25°C) with a 12-hour light/dark cycle, having free access to food and water.

ADSCs were isolated and cultured using the collagenase digestion and adherence method. Two-week -old male SPF-grade SD rats were euthanized by cervical dislocation and then immersed in alcohol for 5 minutes for disinfection. Under a sterile hood, adipose tissue from the bilateral inguinal regions of the rats was excised and placed in a 10 cm sterile culture dish. The tissue was washed three times with PBS to remove fascia and blood vessels. The adipose tissue was minced as finely as possible, and an equal volume of preheated 0.1% type I collagenase was added. The mixture was then shaken and digested at 37°C for 1 hour on a constant temperature shaker until the tissue became chylous. Digestion was terminated by adding an equal volume of α-MEM medium containing 10% foetal bovine serum (Gibco, USA) and 1% penicillin/streptomycin (HyClone, USA). The mixture was repeatedly pipetted to disperse the digested adipose tissue as much as possible. Undigested adipose tissue was filtered out using a 70 μm sieve. The filtered liquid was centrifuged at 1000 rpm for 5 minutes, and the upper fat layer and supernatant were discarded. The precipitated cells were washed once with PBS (1000 rpm, 5 minutes) and resuspended in α-MEM medium containing 10% foetal bovine serum and 1% penicillin/streptomycin. The cells were then seeded into cell culture flasks and placed in a cell incubator for cultivation. It is crucial to avoid moving the culture flasks to prevent disrupting cell adherence. The medium was first changed after at least 2–3 days, and thereafter every 2–3 days until the cells reached 80%-90% confluence

for passage. To identify the extracted cells, flow cytometry was used to detect the cell surface markers CD29, CD34, CD44, and CD45.

The osteogenic differentiation of ADSCs was induced with a medium containing 10% FBS, 1% PS, dexamethasone (10^-8 mol/L), ascorbic acid (50 μg/ml), and β-glycerophosphate (10^-2 mol/L) in α-MEM. The components were prepared as follows: Dexamethasone (3.925 mg in 1 ml EtOH) was diluted to 10^-4 mol/L and stored at −20°C, adding 10 μl/100 ml medium. Ascorbic acid (500 mg in 10 ml medium) was filtered, aliquoted, and stored at −20°C, adding 100 μl/100 ml medium. β-Glycerophosphate (4.32 g in 10 ml medium) was similarly prepared, stored, and added at 0.5 ml/100 ml medium. All solutions were kept in the dark. ADSCs were induced for osteogenic differentiation using the designated osteogenic induction medium. After 7 days of induction, Alkaline phosphatase (ALP) staining and ALP activity quantification were performed to evaluate early osteogenic capacity. After 21 days of induction, Alizarin Red S (ARS) staining was conducted to assess late-stage osteogenic differentiation.

Cell transfection

To knock down the Atoh8 gene, we opted to use siRNA from GenePharma. The sequences were GCCUGUAACUACAUCCUGUTT ACAGGAUGUA GUUACAGGCTT (si-atoh8–1242), CUCGUCAAUUU CACACGUATT UACGUGUGAAAUUGACGAGTT (si-atoh8–995), and CUUUCCGAUUGGACUUGGATT UCCAAGUCCAAUCGGAAAGTT (si-atoh8–541). ADSCs were cultured in an incubator maintained at 2% O2, 5% CO2, and 37°C. Once the ADSCs reached 60%-70% confluence in appropriate well plates, Lipofectamine 3000 (Invitrogen, Waltham, MA, USA) was used to transfect atoh8 siRNA (si-atoh8) or non-targeting siRNA as a negative control (si-nc), following the manufacturer's protocol. After 24 hours of transfection, cells were washed with PBS, and the medium was replaced with complete medium for subsequent experiments. Total RNA was extracted 24 hours post-transfection for qRT-PCR analysis of atoh8 to determine the transfection efficiency in ADSCs across groups.

Cell sheet formation

In this experiment, an osteogenic induction medium was used to induce ADSCs cultured in six-well plates to form cell sheets. The osteogenic induction medium was prepared by adding ascorbic acid (50 μg/ml) to α-MEM medium containing 10% foetal bovine serum and 1% penicillin-streptomycin, and stored in the dark.

Establishment and intervention of bone defect models

Two types of bone defect models were established, each with two groups: (1) si-nc group: SD rats with bone defects were implanted with ADSC sheets transfected with non-targeting siRNA. (2) si-atoh8–1242 group: SD rats with bone defects were implanted with ADSC sheets transfected with si-Atoh8–1242.

The critical-sized calvarial bone defect model in SD rats is a common method for studying bone regeneration and repair. It is generally accepted that bone defects ≥5 mm in diameter do not completely heal within the lifespan of rats, thus qualifying as critical-sized bone defects. Some researchers suggest that ≥8 mm defects may be a more stringent criterion. Considering the calvarial size of 4-week-old rats and the limited 4-week intervention period in this study, we opted for the classical method to create a 5 mm circular critical-sized calvarial bone defect [18,19]. Four-week-old male SD rats ($n = 7$ per group), weighing approximately 100–150 grams, were anesthetized with isoflurane. Rats were placed in an anaesthesia chamber with an initial concentration of 4–5%, and once unconscious, the concentration was reduced to 1–2% to maintain anaesthesia throughout the surgery. Isoflurane was continuously supplied through an anaesthesia mask to ensure the rats remained anesthetized. After anaesthesia, rats were fixed on the surgical table, and the head region was shaved and disinfected. Sterile techniques were used to ensure the cleanliness of the surgical area and instruments. A longitudinal incision was made along the midline of the rat's skull to expose the cranium. A circular defect with a diameter of 5 mm was created in the centre of the rat's skull using a surgical trephine, taking care not to damage the dura mater. The defect was created to fully penetrate the skull but not injure the underlying brain tissue. Cell sheets were implanted into the defects according to the groups. After surgery, the skin was sutured, and antibiotics were administered to prevent infection. In this experiment, metronidazole sodium chloride injection was administered intraperitoneally for 3 days post-surgery. Metronidazole was administered at 15 mg/kg body weight, twice daily. Rats were housed individually, and the environment was kept clean. The rats' health status and wound healing were regularly observed. Rats were euthanized 4 weeks after intervention, and skulls were collected for radiological and histological analysis.

Diagrams of the surgical procedure are presented in Supplementary Figure A.

For the femoral defect model, 6-week-old male SD rats ($n = 3$ per group), weighing approximately 200–250 grams, were anesthetized with 1% pentobarbital solution (45 mg/kg rat weight). After shaving and disinfecting the knee joint and femur, a lateral incision was made to expose the femoral condyle and distal femoral diaphysis. A hole was drilled parallel to the long axis of the femur at the femoral condyle, and the presence of a hollow sensation accompanied by bleeding indicated that the cancellous bone had been reached, creating a hemispherical defect with a radius of approximately 2 mm. Cell sheets were implanted into the defects according to the groups. After surgery, the skin was sutured, and the antibiotic prophylaxis protocol for infection prevention followed the same regimen as that used in the critical-sized calvarial bone defect model. Rats were euthanized 4 weeks after intervention, and femurs were collected for radiological and histological analysis. Diagrams of the surgical procedure are presented in Supplementary Figure B.

Micro-CT analysis

The specimens were fixed in 4% paraformaldehyde for 24 to 48 hours ($n = 3$ per group) and underwent micro-computed tomography (Siemens Inveon, Erlangen, Germany) to determine changes in the tissue surrounding the implants. Specifically, the calvarial bone defect model underwent 3D reconstruction of a 5 mm diameter circle at the site of the calvarial defect, while the femoral bone defect model underwent 3D reconstruction of a 2 mm × 2 mm × 2 mm area at the defect site. Morphometric parameters of the bone surrounding the defect were analysed, including bone volume/total volume (BV/TV, %), bone surface area/bone volume (BS/BV, 1/mm), mean trabecular thickness (TbTh, mm), mean trabecular number (TbN, 1/mm), and mean trabecular separation (TbSp, mm).

Histological analysis

Decalcified tissue sections were stained with haematoxylin and eosin (HE), Masson's trichrome, and safranin O-fast green to observe new bone formation.

Cell proliferation assay

Cells were seeded in 96-well plates with 100 μL of cell suspension added to each well, typically at a concentration of 5 × 10^3 cells/well. The cells were cultured for 24 hours in a 37°C, 5% CO2 incubator to allow adherence. Cells were then treated according to the experimental objectives. Cell proliferation at 0, 24, 48, and 72 hours was detected using a Cell-counting kit-8 (CCK-8; 10 μl per well; PCM, Xi'an, China). The absorbance (OD value) of each well was measured at 450 nm using a microplate reader (Thermo Fisher Scientific, Waltham, MA, USA). The number of cells is directly proportional to the OD value, with a higher OD value indicating a greater number of cells.

Scratch healing assay

Cells were seeded in 6-well plates at approximately 5 × 10^5 cells per well and cultured in a 37°C, 5% CO2 incubator to allow adherence and formation of a monolayer, reaching approximately 90% confluence. Different treatments were applied according to the experimental design. A straight line was scratched perpendicular to the monolayer surface using a sterile pipette tip (200 μL tip) to create a wound. Floating cells were gently washed away with PBS to ensure a clear wound. Cells were cultured in serum-free α-MEM, and images were captured after 12 hours.

Transwell migration assay

A 24-well plate with Transwell inserts (pore size 8.0 μm; Corning-Costar) was prepared. 200 μL of cell suspension containing approximately 2 × 10^5 cells was added to the upper chamber of the Transwell insert. 600 μL of medium containing 10% FBS was added to the lower chamber as a chemoattractant. The 24-well plate was incubated in a 37°C, 5% CO2 incubator for 24–48 hours to allow cell migration. After incubation, non-migrated cells in the upper chamber were gently removed with a cotton swab. Migrated cells on the lower surface were fixed with 4% paraformaldehyde for 20 minutes and stained with 0.1% crystal violet for 10 minutes. Images were captured under a microscope, and quantitative results were obtained by measuring the absorbance at 570 nm after dissolving the stain in 500 μl of 33% acetic acid.

ALP and ARS

ALP activity was quantitatively measured using the ALP assay kit (Jiancheng, Nanjing, China) following the manufacturer's protocol, and the BCIP/NBT alkaline phosphatase colorimetric kit (Beyotime Biotech, Shanghai, China) was employed for the detection. Calcium deposition was examined through staining with 2% Alizarin Red S (Solarbio, Beijing, China).

Cell adhesion assay

Prior to the cell adhesion assay, titanium disks of 12 mm diameter and 2 mm thickness were prepared, soaked in 5 ml of 95% ethanol for 48 hours, and thoroughly disinfected via UV irradiation. Transfected ADSCs (3 × 10^3/well) were centrifuged and seeded onto 24-well culture plates, with a titanium disk placed in each well. After 24 hours, the culture medium was removed, and the titanium disk samples were washed three times with PBS buffer. Subsequently, the samples were fixed with 4% paraformaldehyde for 10 minutes at room temperature. Following permeabilization, cells were stained using a dual-fluorescence staining method: the cytoskeleton was labelled with F-actin dye (green), and the cell nuclei were stained with DAPI (blue). Finally, the number of adherent cells, the morphology, and the spreading of ADSCs were observed using a confocal laser scanning microscope (OLYMPUS, Tokyo, Japan).

Quantitative real-time PCR

To determine the relative expression levels of Atoh8, ALP, RUNX2, Col-1, BMP2, RANKL, and OPG mRNA in ADSCs, the following steps were taken for the quantitative real-time PCR experiment: 1 × 10^6 ADSCs per well were seeded onto 6-well culture plates and incubated under different treatment conditions for 24 hours to ensure sufficient cellular response to the treatment. Total RNA was extracted from the treated cells using an appropriate RNA extraction kit (e.g. TRIzol), following the manufacturer's instructions to ensure RNA purity and integrity. Reverse transcription of the extracted RNA was performed using the SYBR Premix ExTaq II kit (TaKaRa, Tokyo, Japan) to synthesize cDNA, following the kit's instructions for reaction conditions. qRT-PCR analysis was conducted using the StepOne Plus Real-Time PCR System (Applied Biosystems, Foster City, CA, USA). Each reaction mixture contained cDNA template, SYBR Premix ExTaq II, specific primers, and nuclease-free water, with a total volume of 20 µL. The PCR reaction programme was set as follows: initial denaturation at 95°C for 30 seconds, followed by 40 cycles of 95°C for 5 seconds and 60°C for 30 seconds. The relative expression levels of each target mRNA were calculated using the 2−ΔCT method. GAPDH served as the internal reference gene for normalizing the expression levels across samples. All primers used in this study were synthesized by Sangon Biotech (Shanghai), and the detailed sequences are provided in Supplementary File 1: Table 1.

Protein extraction and western blotting

Cells were seeded in 100 mm dishes and cultured in a 37°C, 5% CO2 incubator until they reached 90% to 100% confluence. Following incubation under different treatment conditions for 24 hours, the culture medium was removed, and the cells were gently washed with cold PBS. RIPA buffer (ZHHC, China) was added to lyse the cells. After incubation on ice for 30 minutes with gentle shaking to ensure complete lysis, the lysate was transferred to a centrifuge tube and centrifuged at 12,000 rpm for 15 minutes at 4°C. The supernatant, containing the total protein solution, was collected. The protein concentration was quantified using the BCA Protein Assay Kit (Beyotime Biotechnology, China) according to the kit's instructions. Based on the protein concentration, protein samples were mixed with 5×SDS-PAGE sample buffer to a total volume of 10 µl to 20 µl and heated at 95°C for 5 minutes. The samples were then loaded onto SDS-PAGE gels for electrophoretic separation. Proteins were transferred from the gel to a PVDF membrane using the wet transfer method. The PVDF membrane was blocked with 5% skimmed milk powder or BSA for 1 hour at room temperature. The membrane was incubated overnight at 4°C with the following primary antibodies: anti-GAPDH (1:1000, ab181602), anti-RUNX2 (1:2000, ab236639), anti-BMP2 (1:2000, ab284387) (all from Abcam Biotechnology, MA, USA) and anti-ATOH8 (Signalway Antibody, Maryland, USA). The PVDF membrane was washed three times with TBS-T (TBS buffer containing 0.1% Tween-20) for 5 minutes each at room temperature. The membrane was then incubated with HRP-conjugated secondary antibodies (Boster, Wuhan, China) for 1 hour at room temperature. After three additional washes with TBS-T for 5 minutes each, the membrane was visualized using a chemiluminescent substrate (ECL) and a chemiluminescent imaging system (Bio-Rad GelDoc XR+, Hercules, CA, USA). ATOH8 and

Table 1. Primer sequences used in qRT-PCR to detect ADSC genes.

ADSC genes	Forward primer 5′→3′	Reverse primer 5′→3′
Atoh8	TCCAGCCATCCAGGGTTACT	TTGGCTTGAGGTGGACTTGG
GAPDH	CAAGTTCAACGGCACAGTCA	CCATTTGATGTTAGCGGGAT
ALP	CAACGAGGTCATCTCCGTGATG	TACCAGTTGCGGTTCACCGTGT
RUNX2	CCCAGTATGAGAGTAGGTGTCC	GGGTAAGACTGGTCATAGGACC
Col-1	TGTTGGTCCTGCTGGCAAGAATG	GTCACCTTGTTCGCCTGTCTCAC
BMP2	GAGGAGAAGCCAGGTGTCT	GTCCACATACAAAGGGTGC
OPG	CACGAGCCTTATCCCATTTG	CATAACCTACCCCTGCTTGTCT
RANKL	TCAGCCGTTTGCTCACCTC	TTAACCCTTAGTTTTCCGTTGC

GAPDH were located at the same kDA. The blot membrane was incubated with stripping buffer (NCM Biotech, Suzhou, China) at room temperature with moderate shaking for 10 minutes to remove the antibody. The intensity of the protein bands was observed, with GAPDH serving as the internal reference protein. The original Western Blot images are presented in Supplementary Figure C.

Statistical analysis

Quantitative data are presented as mean with upper and lower limits, and graphs were generated using GraphPad Prism 8.0 software (GraphPad Software, San Diego, CA, USA). Data from repeated measurements were analysed using t-test. All statistical analyses were conducted with a significance level set at 0.05. A P-value less than 0.05 was considered statistically significant. And all experiments were repeated at least three times.

Results

Knockdown of Atoh8 expression in ADSCs via liposome transfection

The primary objective of the experiments was to extract cells and validate the ability of siRNA to knockdown atoh8 in ADSCs. First, ADSCs were isolated from the inguinal region of SD rats, and the characteristics of the cultured ADSCs were verified using flow cytometry. The results showed that the cells were positive for mesenchymal stem cell markers CD29 and CD44. Concurrently, both CD34 and CD45 were negative in the in vitro cultured cells, indicating that the isolated cells retained ADSC properties (Figure 1(a)). The extracted ADSCs possessed multidirectional differentiation potential, and their adipogenic potential was confirmed through adipogenic induction (Figure 1(b)). Subsequent experiments also validated their osteogenic potential. Three different siRNAs (si-atoh8–541, si-atoh8–995, si-atoh8–1242) were designed to intervene in ADSCs, and their ability to knockdown atoh8 was determined by qRT-PCR post-transfection. Among them, the si-atoh8–1242 group demonstrated the highest knockdown efficiency compared to the control group (Figure 1(c)). The western blot results confirmed that Atoh8 protein levels in ADSCs were relatively downregulated after transfection with si-atoh8–1242 (Figure 1(d)). Consequently, si-atoh8–1242 was selected for subsequent cellular interventions.

Enhanced bone defects repaired capability in SD rats following knockdown of Atoh8 expression in ADSCs

We first conducted animal experiments to investigate the impact of Atoh8 on the ability of adipose-derived stem cells to intervene in and repair bone defects in vivo. An extreme bone defect model was established in the skull of 4-week-old male SD rats (Figure 2(a, b)), and micro-CT analysis and histological evaluation were performed to determine the extent of the intervention's effects. In the skull extreme bone defect model, the si-atoh8–1242 group exhibited significantly higher bone volume/total volume (BV/TV, %) at the defect site. The bone surface/bone volume (BS/BV, 1/mm) was significantly lower in the si-atoh8–1242 group, indicating denser newly formed bone. Additionally, the mean trabecular thickness (TbTh, mm) was significantly increased in the si-atoh8–1242 group, while mean trabecular number (TbN, 1/mm) and mean trabecular spacing (TbSp, mm) showed similar trends, with the si-atoh8–1242 group displaying more trabeculae and smaller trabecular spacing (Figure 2(c)). For the dissected skulls, HE staining, Masson's trichrome staining,

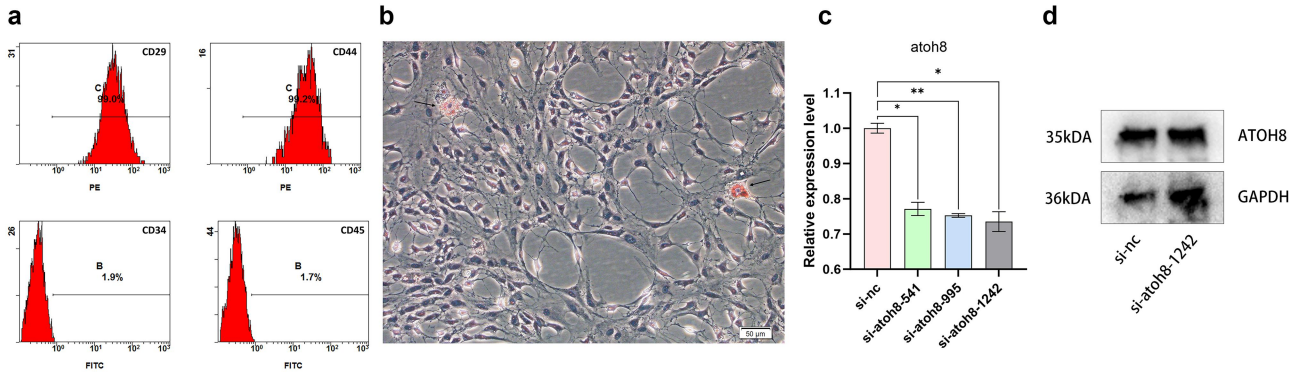

Figure 1. (a) Cells were isolated from adipose tissues of inguinal region in 2-week-old male SD rats, which were identified as ADSCs by flow cytometry. (b) Microscopic observation of ADSCs after 14 d of adipogenic induction. Arrows indicate lipid droplets. Scale bar = 50 μm. (c) Relative expressions of Atoh8 were detected after 24h of transfection with empty vector and three si-RNA liposomes by qRT-PCR. *$p \leq 0.05$, **$p \leq 0.01$. (d) Relative expressions of Atoh8 were detected after 24h of transfection with empty vector and si-atoh8–1242 liposomes by western blotting.

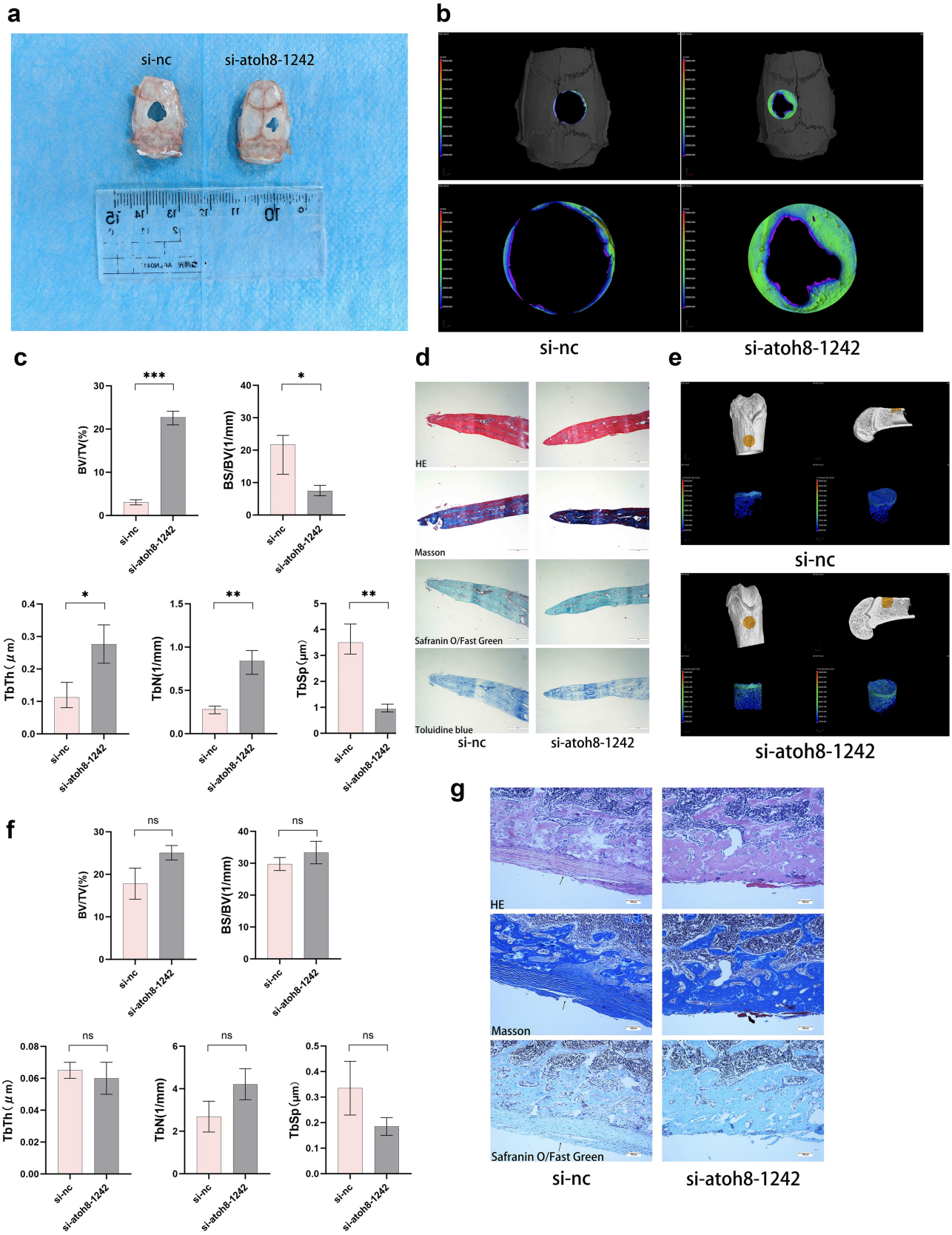

Figure 2. (a) Anatomical results of critical-sized calvarial bone defect model of the SD rats after 4 weeks of intervention. (b) CT 3D reconstruction results of critical-sized calvarial bone defect model of the SD rats. (c) Trabecular bone parameters of critical-sized calvarial bone defect model of the SD rats. *$p \leq 0.05$, **$p \leq 0.01$, ***$p \leq 0.001$. (d) HE and Masson's staining results of critical-sized calvarial bone defect model of the SD rats, safranin O/Fast green, and toluidine blue stainings. Scale bar = 500 μm. (e) CT 3D reconstruction results of the femoral bone defect model of the SD rats. (f) Trabecular bone parameters of critical-sized calvarial bone defect model of the SD rats. ns means not significant. (g) HE, Masson's trichrome, and safranin O/Fast green stains of femoral bone defect model of the SD rats. Arrows indicate non-bone structures. Scale bar = 100 μm.

and Safranin O-Fast Green staining further confirmed the new bone formation in the bone defect model of the si-atoh8–1242 group. HE staining of the si-atoh8–1242 group showed that newly formed bone tissue filled most of the defect area, with distinct trabecular bone structures and higher density, while the si-nc group had less new bone tissue and a significant amount of void space in the defect area. Masson's trichrome staining revealed significantly higher collagen fibre deposition in the si-atoh8–1242 group, indicating higher bone tissue formation and maturity. In contrast, the si-nc group had less collagen fibre deposition and sparser new bone formation. Safranin O-Fast Green staining of the si-atoh8–1242 group showed a large amount of newly mineralized bone tissue with high mineralization. In contrast, the si-nc group had less mineralized bone tissue with lower mineralization (Figure 2(d)). Similar results were obtained when validating the femoral defect model. Microscopic observations of soft tissue sections after staining revealed that the bone surface of the control group was covered with non-bone structures, suggesting that knockdown of Atoh8 not only enhanced osteogenic differentiation of ADSCs but also inhibited their differentiation into other cell types (Figure 2(e–g)). In summary, the si-Atoh8–1242 group demonstrated significantly superior bone regeneration compared to the si-nc group in the critical-sized calvarial bone defect model. However, in the femoral defect model, although bone morphometric parameters still indicated an enhancement in bone repair capacity in the si-Atoh8–1242 group, the improvement was less pronounced than that observed in the calvarial defect model. These results indicate that ADSCs with knocked down Atoh8 have better abilities to promote bone regeneration and repair.

In vitro experiments showed that knocking down Atoh8 expression in ADSCs reduced their proliferation and migration abilities

To investigate the effects of knocking down Atoh8 on the proliferation ability of ADSCs from SD rats, we first conducted the following experiments in vitro. Proliferation, as one of the basic life activities of cells, was assessed using the CCK-8 assay to examine the impact of Atoh8 knockdown on ADSC proliferation. By measuring the proliferation abilities of the experimental and control groups at different time points (0, 24, 48, 72 hours), we found that knocking down Atoh8 significantly reduced the proliferation ability of ADSCs (Figure 3(a)). Subsequently, we performed a 24-hour Transwell migration assay, followed by quantitative analysis using crystal violet staining, which revealed that knocking down Atoh8 also significantly reduced the migration ability of ADSCs (Figure 3(b,c)). Similar conclusions were drawn from the 12-hour scratch assay analysis, showing a significant decrease in scratch healing ability in the Atoh8-knockdown group (si-atoh8–1242 group) (Figure 3(d)). We used smooth metal titanium sheets as the substrate for cell adhesion and transferred liposome-transfected ADSCs onto the titanium sheets for cell culture. The results showed that the number of adhered cells in the experimental group was lower than that in the control group, but the cell morphology in the experimental group was more ductile (Figure 3(e,f)).

In vitro experiments showed that knocking down Atoh8 expression in ADSCs increased their osteogenic differentiation ability

Next, we examined the effect of knocking down Atoh8 on the osteogenic ability of ADSCs. After culturing the in vitro isolated ADSCs in osteogenic induction medium for 7 days, staining results indicated that the osteogenic ability of ADSCs in the experimental group was significantly improved (Figure 4(a)). Correspondingly, measurements of cells at the same time point revealed an increase in ALP content in the experimental group (Figure 4(b)). Alizarin Red staining results showed similar findings at 21 days (Figure 4(c)). To investigate the effect of Atoh8 knockdown on the expression of osteogenic and osteoclastogenic markers in ADSCs, we performed qRT-PCR and Western blot analyses. The results showed significant changes in the expression levels of key osteogenic and osteoclastogenic genes. Among them, the mRNA levels of osteogenic-related key genes Runx2, Alp, Col1, and Bmp2 were upregulated. Rankl, a crucial regulator of osteoclastogenesis, showed significantly downregulated mRNA expression in the experimental group, while Opg, a decoy receptor for Rankl, showed a slight increase in expression in the experimental group. These changes led to a decrease in the Rankl/Opg ratio, suggesting a possible reduction in osteoclastogenic activity (Figure 4(d)). The changes in protein levels were consistent with the mRNA expression data (Figure 4(e)), further supporting the conclusion that knocking down Atoh8 can enhance osteogenic differentiation of ADSCs.

Discussion

In the current study, the Atoh8 inhibition demonstrated significantly better bone repair in both, the skull and femoral defect models. Likewise, the in vitro

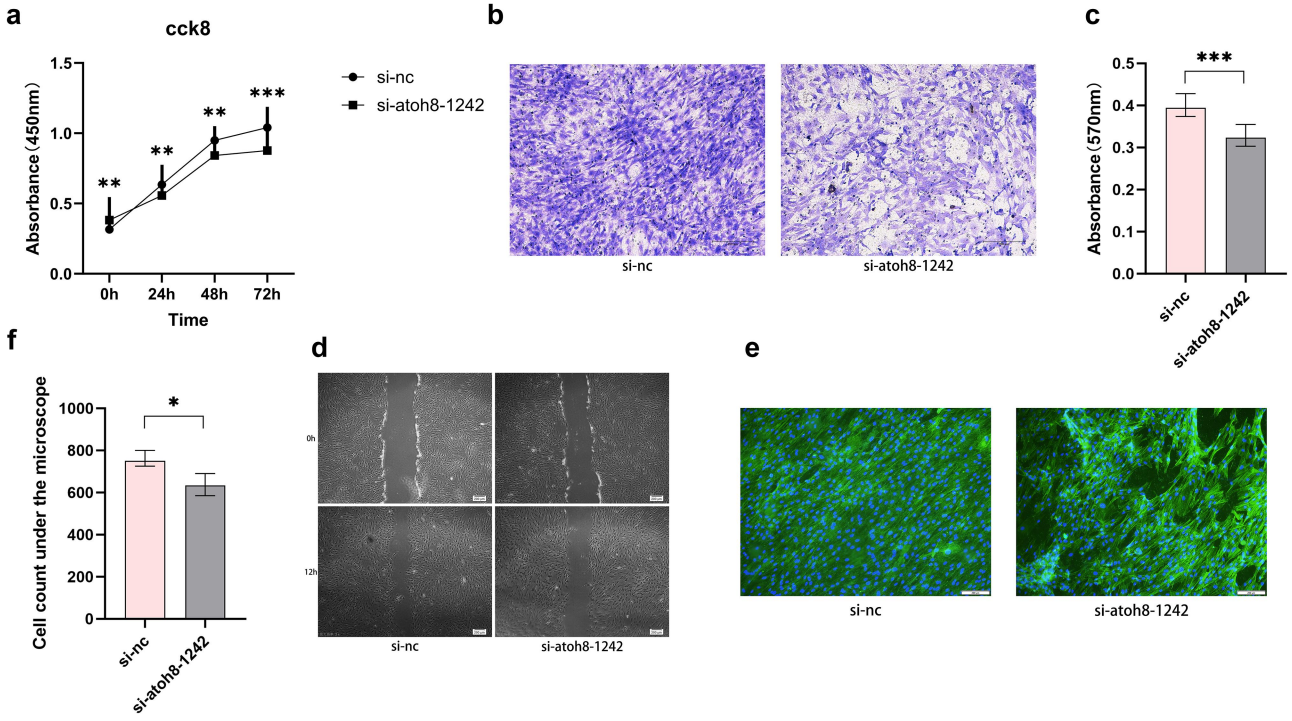

Figure 3. (a) CCK-8 results at 0, 24, 48, and 72 h after transfection with empty vector or si-Atoh8–1242 for 24 h. $^{**}p \leq 0.01$, $^{***}p \leq 0.001$. (b) Transwell assay and crystal violet staining 24 h after transfection with empty vector or si-Atoh8–1242 for 24 h. Scale bar = 200 μm. (c) Absorbance at 570 nm after crystal violet was dissolved in 500μl 33% acetic acid. $^{***}p \leq 0.001$. (d) Scratch test 12 h after transfection with empty vector or si-Atoh8–1242 for 24 h. Scale bar = 200 μm. (e) Double fluorescence staining 24 h after it was seeded on titanium disks following transfection with empty vector or si-Atoh8–1242 for 24 h. Scale bar = 200 μm. (f) Quantitative results of adhered cell count. $^{*}p \leq 0.05$.

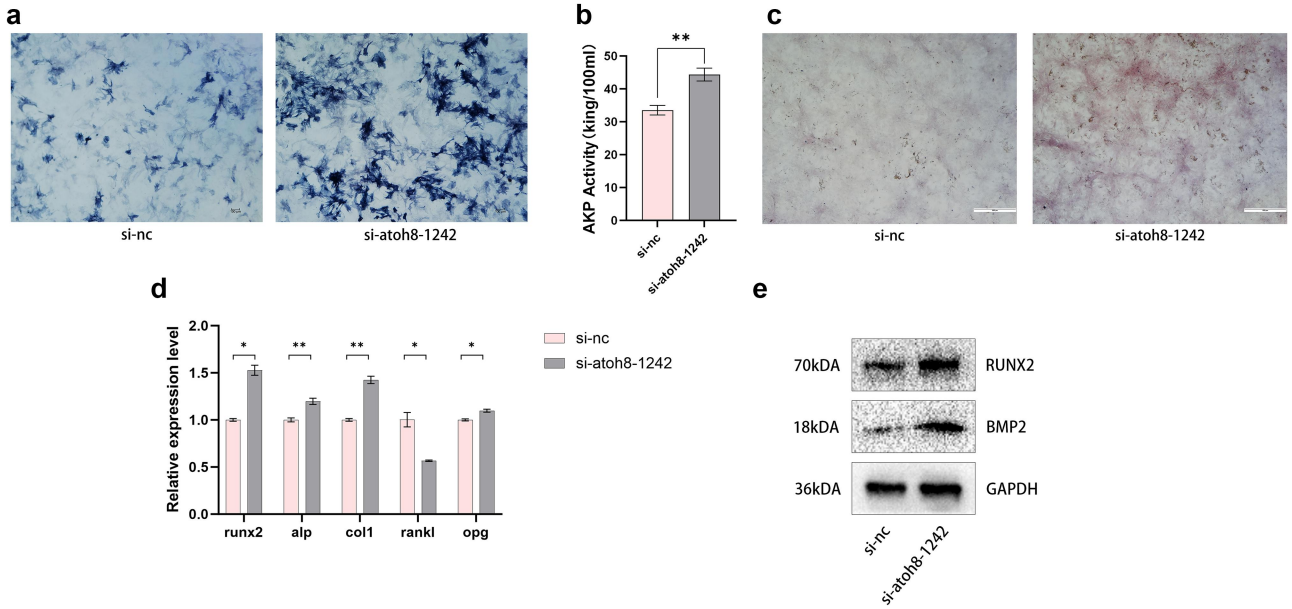

Figure 4. (a) Osteogenic induction culture started 24 h after transfection with empty vector or si-Atoh8–1242, followed by ALP staining after 7 d. Scale bar = 100 μm. (b) quantitative ALP results. $^{**}p \leq 0.01$. (c) Osteogenic induction culture started 24 h after transfection, followed by Alizarin Red staining after 21 d. Scale bar = 500 μm. (d) RNA was extracted from cells 24 h after transfection. Specific gene expressions were analyzed by qRT-PCR. $^{*}p \leq 0.05$, $^{**}p \leq 0.01$. (e) RNA was extracted from cells 24 h after transfection. Specific gene expressions were detected by Western blotting.

experiments also showed that the knock down of Atoh8 expression reduced the proliferation and migration but increased osteogenic differentiation ability of ADSCs.

Multiple types of adult stem cells have been proven to have potential applications in bone tissue engineering [20,21]. However, among other adult stem cells, the most notable feature of adipose-derived stem cells (ADSCs) is their abundant presence in the human body and their easier accessibility compared to other adult stem cells. The number of stem cells obtained from adipose tissue is at least 500 times greater than that obtainable from equivalent bone marrow tissue [22–24]. ADSCs have also revealed various matrices in the process of bone regeneration. They possess multipotency, enabling them to differentiate into osteoblasts under specific inductive conditions, directly participating in bone tissue formation and repair [25]. Additionally, ADSCs can secrete various angiogenic factors and extracellular matrix components to promote bone regeneration, as well as immune regulatory factors to modulate inflammatory responses, creating a microenvironment conducive to bone regeneration [26–28]. Nevertheless, the clinical application of ADSCs in bone tissue engineering still faces the challenge of suboptimal osteogenic differentiation ability.

Given the scarcity of research on this gene in relation to ADSCs, we have yet to retrieve relevant literature. Therefore, we conducted in vitro and in vivo experiments to verify the correlation between Atoh8 expression and the osteogenic capacity of ADSCs. Our findings indicate that Atoh8 expression is indeed negatively correlated with osteogenic capacity, suggesting that targeting Atoh8 through genetic intervention may serve as a novel strategy to enhance ADSC-mediated bone tissue engineering for the treatment of bone defects. This study chose to investigate the effect of Atoh8 knockdown on the osteogenic capacity of ADSCs by establishing a critical-size calvarial bone defect model in SD rats for the following reasons: The critical-size bone defect model in experimental animals is defined as the smallest bone gap in a specific bone that fails to heal spontaneously throughout the experimental period or exhibits a bone regeneration rate below 10% throughout the animal's lifetime [29]. This model serves as an ideal platform for evaluating novel bone repair materials and techniques, as any observed bone regeneration can be attributed solely to the tested intervention rather than natural healing processes. Additionally, SD rats possess moderate body size, good breeding ability, ease of handling, and their behavioural, physiological, genetic, and cognitive characteristics are similar to humans, enhancing the clinical relevance of our research findings [30]. By utilizing a standardized critical-size bone defect model, the results across different studies are highly comparable, facilitating the validation and comparison of various bone regeneration strategies. Furthermore, to validate the effect of Atoh8 knockdown on the osteogenic capacity of ADSCs, we also established a bone defect model in the femur of SD rats. The femur was chosen as the second experimental model due to its differences in bone remodelling mechanisms compared to the skull, providing a distinct biological environment that contributes to a comprehensive assessment of the role of Atoh8 knockdown in osteogenesis. Repeating the validation in different anatomical sites eliminates potential confounding factors associated with a single model, enhancing the reliability of our experimental results. The combination of the femoral defect model with the calvarial model better simulates clinical scenarios, rendering our research findings more applicable and informative. By observing similar trends of enhanced osteogenesis in bone defect models at two different sites, we further confirmed that Atoh8 knockdown significantly enhances the osteogenic capacity of ADSCs. This discovery not only provides new evidence for the potential application of Atoh8 in bone tissue engineering but also lays a solid foundation for future clinical translational research.

Our in vitro experimental results also demonstrate that Atoh8 negatively regulates osteogenic differentiation in ADSCs. Knockdown of Atoh8 significantly upregulates the expression of multiple osteogenic markers while downregulating the expression of the osteoclast marker Rankl, resulting in a decreased Rankl/Opg ratio. This verifies the enhancing effect of Atoh8 knockdown on osteogenic differentiation in ADSCs and its potential inhibitory effect on osteoclastogenesis. These findings are significant for understanding the osteogenic mechanisms of ADSCs and developing therapeutic strategies for bone-related diseases. Osteogenic differentiation of ADSCs is regulated by various genes, including ERK, Wnt, and Notch signalling pathways [31–33]. ALP and Col1 are essential components of bone matrix produced by osteoblasts [34]. BMPs, particularly BMP2, 4, 6, 7, and 9 among the 16 subtypes, are potent inducers of osteogenic differentiation in adipose-derived stem cells [35]. BMPs are also crucial regulators of osteogenic differentiation, promoting the expression of osteogenic genes through the activation of the Smad signalling pathway [36]. BMP-activated Smads induce the expression of Runx2, which forms a complex with itself to initiate the expression of osteoblast-specific genes [37–39]. Runx2 regulates the expression of a series of osteoblast-specific genes, including type I collagen, bone sialoprotein,

osteocalcin, and osteopontin [40–42]. Our study further found that Atoh8 knockdown significantly reduced the Rankl/Opg ratio. The Rankl (receptor activator of nuclear factor-κB ligand) and Opg (osteoprotegerin) system also plays a vital role in bone metabolism. Rankl, produced by osteoblasts and other stromal cells, promotes osteoclastogenesis, activation, and survival by binding to Rank (receptor activator of nuclear factor-κB). In contrast, Opg, a decoy receptor for Rankl, inhibits osteoclast formation and activity by binding to Rankl, thereby preventing its interaction with Rank [43,44]. By modulating the balance between Rankl and Opg, bone resorption and formation processes can be regulated, affecting bone remodelling and repair [45]. The decreased Rankl/Opg ratio suggests reduced osteoclastogenesis activity, further supporting the positive regulatory role of Atoh8 in bone resorption.RR

Interestingly, we have found that knocking down the Atoh8 gene significantly reduced cell proliferation but enhanced the osteogenic capacity of cells. Through literature review, we have found similar findings where certain genes or interventions exerted differential effects on stem cell proliferation and osteogenic differentiation. For instance, CMTM8 negatively regulated the osteogenic differentiation of BMSCs while promoting their proliferation [46]. Notch1 inhibition significantly reduced BMSCs proliferation but enhanced osteogenic differentiation [47]. Besides, uniaxial mechanical stretch promoted the proliferation of dental pulp stem cells while suppressing their osteogenic differentiation [48]. Some studies have reported consistent effects. For example, TGF-β3 inhibited both osteogenic differentiation and proliferation in hMSCs [49]. Notably, previous researches have demonstrated that in Atoh8-KO myoblasts, AKT phosphorylation levels were significantly reduced whereas the overexpression of Atoh8 increased AKT phosphorylation [50]. Since the AKT signalling pathway is a key regulator of cell proliferation [51], a similar mechanism may be occurring in Atoh8-knockdown ADSCs, leading to the observed reduction in proliferation.

The current study has limitation. Although this study reveals the effects of Atoh8 knockdown on cell proliferation and osteogenesis, the specific molecular mechanisms remain unclear. Future studies will further explore the mechanisms by comprehensively analysing changes in the gene expression profile of cells after Atoh8 knockdown using gene sequencing technology, aiming to identify potential regulatory pathways and target genes. This will help to elucidate the specific mechanisms of Atoh8 in cell proliferation and osteogenesis. Gene sequencing can not only help identify key genes regulated by Atoh8 but also construct potential signalling pathway network models through bioinformatics analysis. Subsequently, functional validation experiments, such as gene knockout or overexpression, and the use of signalling pathway inhibitors or agonists, can further confirm the roles of these pathways and genes in Atoh8 regulation. From a clinical perspective, knocking down Atoh8 in ADSCs offers a novel strategy for bone defect repair, as enhancing osteogenic differentiation is crucial for accelerating bone healing and improving bone tissue quality. Therefore, further in vivo studies and preclinical research are required to evaluate the efficacy and safety of Atoh8-knockdown ADSCs in large animal models, providing essential groundwork for future clinical translation.

Conclusion

In summary, the current research results indicate that knocking down Atoh8 promotes the osteogenic differentiation ability of ADSCs in vitro and in vivo, thereby accelerating the repair of bone defects. This study further reveals the clinical potential of ADSCs in tissue engineering bone defect repair and characterizes the role of Atoh8 in the osteogenic differentiation of ADSCs.

Abbreviations

bHLH	qbasic helix-loop-helix
MSCs	mesenchymal stem cells
BMSCs	bone marrow mesenchymal stem cells
ADSCs	adipose-derived stem cells
SD rats	Sprague Dawley rats
CT	computed tomography
3D	3-dimensional
BV/TV	bone volume/total volume
BS/BV	bone surface area/bone volume
TbTh	mean trabecular thickness
TbN	mean trabecular number
TbSp	mean trabecular separation
CCK-8	cell-counting kit-8
HE	haematoxylin and eosin
ARS	alizarin Red S
ALP	alkaline phosphatase
RUNX2	runt-related transcription factor 2
COL-1	type I collagen
BMP2	bone morphogenetic protein-2
OPG	osteoclastogenesis inhibitory factor
RANKL	receptor activator for nuclear factor-κ B ligand
qRT-PCR	quantitative real-time PCR
GAPDH	glyceraldehyde-3-phosphate dehydrogenase

Disclosure statement

No potential conflict of interest was reported by the author(s).

Funding

The author(s) reported there is no funding associated with the work featured in this article.

Author contributions statement

Zian Yi contributed to the design and conception of the study, participated in the entire experimental process, and was involved in drafting and revising the manuscript. Shuang Song and Yuxin Bai performed *in vivo* experiments, including animal handling and bone defect model establishment, and contributed to data analysis. Guanhua Zhang, Yuxi Wang and Zijun Chen performed *in vitro* experiments and interpreted the molecular data related to osteogenic differentiation. Xuefeng Chen and Banglian Deng contributed to the statistical analysis and data interpretation, and assisted in revising the manuscript for intellectual content. Xiangdong Liu provided key guidance on the experimental approach and reviewed the manuscript in detail. Zuolin Jin supervised the overall study design and the experiments and made critical revisions of the manuscript. All authors have read and approved the final work.

Arrive guidelines compliance statement

We confirm that our research has adhered to the ARRIVE guidelines for the reporting of animal research. A checklist has been uploaded as part of the submission.

Data availability statement

The date that support the findings of this study are openly available in 'figshare' at https://doi.org/10.6084/m9.figshare.27800367.v1.

References

[1] GBD. Fracture collaborators. Global, regional, and national burden of bone fractures in 204 countries and territories, 1990–2019: a systematic analysis from the global burden of disease study 2019. Lancet Healthy Longev. 2019;2:e580–92.

[2] Lei Y, Zhang Q, Kuang G, et al. Functional biomaterials for osteoarthritis treatment: from research to application. Smart Med. 2022;1(1):e20220014. doi: 10.1002/SMMD.20220014

[3] Weinand C, Neville CM, Weinberg E, et al. Optimizing biomaterials for tissue engineering human bone using mesenchymal stem cells. Plast Reconstr Surg. 2016;137(3):854–863. doi: 10.1097/01.prs.0000479991.72867.ba

[4] Autelitano L, Meazzini MC. Alveolar cleft reconstruction with vomerine bone: two surgical procedures in one step: a case series. Plast Aesthetic Res. 2023;10:N–A. doi: 10.20517/2347-9264.2022.57

[5] Choi J-W, Kim Y-C. Asian facial recontouring surgery. Plast Aesthetic Res. 2023;10:59. doi: 10.20517/2347-9264.2023.30

[6] Fu X, Liu G, Halim A, et al. Mesenchymal stem cell migration and tissue repair. Cells. 2019;8(8):784. doi: 10.3390/cells8080784

[7] Xu Y, Saiding Q, Zhou X, et al. Electrospun fiber-based immune engineering in regenerative medicine. Smart Med. 2024;3(1):e20230034. doi: 10.1002/SMMD.20230034

[8] Pittenger MF, Mackay AM, Beck SC, et al. Multilineage potential of adult human mesenchymal stem cells. Science. 1999;284(5411):143–147. doi: 10.1126/science.284.5411.143

[9] Horwitz EM, Gordon PL, Koo WKK, et al. Isolated allogeneic bone marrow-derived mesenchymal cells engraft and stimulate growth in children with osteogenesis imperfecta: implications for cell therapy of bone. Proc Natl Acad Sci. 2002;99(13):8932–8937. doi: 10.1073/pnas.132252399

[10] Zuk PA, Zhu M, Mizuno H, et al. Multilineage cells from human adipose tissue: implications for cell-based therapies. Tissue Eng. 2001;7(2):211–228. doi: 10.1089/107632701300062859

[11] Divvela SSK, Saberi D, Brand-Saberi B. Atoh8 in development and disease. Biology (Basel). 2022;11(1):136. doi: 10.3390/biology11010136

[12] Inoue C, Bae S, Takatsuka K, et al. *Math6*, a bHLH gene expressed in the developing nervous system, regulates neuronal versus glial differentiation. Genes Cells. 2001;6(11):977–986. doi: 10.1046/j.1365-2443.2001.00476.x

[13] Balakrishnan-Renuka A, Morosan-Puopolo G, Yusuf F, et al. ATOH8, a regulator of skeletal myogenesis in the hypaxial myotome of the trunk. Histochem Cell Biol. 2014;141(3):289–300. doi: 10.1007/s00418-013-1155-0

[14] Liu F, Song D-Y, Huang J, et al. Long non-coding RNA CIR inhibits chondrogenic differentiation of mesenchymal stem cells by epigenetically suppressing ATOH8 via methyltransferase EZH2. Mol Med. 2021;27(1):12. doi: 10.1186/s10020-021-00272-9

[15] Li Y, Li H, Zhang L, et al. Growth/Differentiation 5 promotes the differentiation of retinal stem cells into neurons via Atoh8. J Cell Physiol. 2019;234(11):21307–21315. doi: 10.1002/jcp.28735

[16] Huang M-F, Shoemaker R, Lee D-F. Bcl11b and Atoh8 coordinate cellular plasticity for reprogramming and transformation. Cell Reprogramming. 2022;24(6):324–326. doi: 10.1089/cell.2022.0128

[17] Yahiro Y, Maeda S, Morikawa M, et al. BMP-induced Atoh8 attenuates osteoclastogenesis by suppressing Runx2 transcriptional activity and reducing the rankl/opg expression ratio in osteoblasts. Bone Res. 2020;8(1):32. doi: 10.1038/s41413-020-00106-0

[18] Sato K, Watanabe Y, Harada N, et al. Establishment of reproducible, critical-sized, femoral segmental bone defects in rats. Tissue Eng Part C Methods. 2014;20(12):1037–1041. doi: 10.1089/ten.tec.2013.0612

[19] Spicer PP, Kretlow JD, Young S, et al. Evaluation of bone regeneration using the rat critical size calvarial defect. Nat Protoc. 2012;7(10):1918–1929. doi: 10.1038/nprot.2012.113

[20] Wang P, Liu X, Zhao L, et al. Bone tissue engineering via human induced pluripotent, umbilical cord and bone marrow mesenchymal stem cells in rat cranium.

Acta Biomater. 2015;18:236–248. doi: 10.1016/j.actbio.2015.02.011

[21] Amini AR, Laurencin CT, Nukavarapu SP. Bone tissue engineering: recent advances and challenges. Crit Rev Biomed Eng. 2012;40(5):363–408. doi: 10.1615/CritRevBiomedEng.v40.i5.10

[22] Mainil-Varlet P, Aigner T, Brittberg M, et al. Histological assessment of cartilage repair: a report by the histology endpoint committee of the international cartilage repair society (ICRS). JBJS. 2003;85:45–57. doi: 10.2106/00004623-200300002-00007

[23] Veronesi F, Maglio M, Tschon M, et al. Adipose-derived mesenchymal stem cells for cartilage tissue engineering: State-of-The-Art in *in vivo* studies. J Biomed Mater Res A. 2014;102(7):2448–2466. doi: 10.1002/jbm.a.34896

[24] Si Z, Wang X, Sun C, et al. Adipose-derived stem cells: sources, potency, and implications for regenerative therapies. Biomed Pharmacother. 2019;114:108765. doi: 10.1016/j.biopha.2019.108765

[25] Balderrama IF, Ferreira R, Leão MP, et al. CLINICAL APPLICATIONS for ORAL BONE REGENERATION with MESENCHYMAL STEM CELLS from ADIPOSE TISSUE: WHAT are the LEVELS of SCIENTIFIC EVIDENCE? Cytotherapy. 2021;23(4):7–8. doi: 10.1016/j.jcyt.2021.02.026

[26] Dziedzic DS, Mogharbel BF, Ferreira PE, et al. Transplantation of adipose-derived cells for periodontal regeneration: a systematic review. Curr Stem Cell Res Ther. 2019;14(6):504–518. doi: 10.2174/1574888X13666181105144430

[27] Alonso-Goulart V, Carvalho LN, Marinho ALG, et al. Biomaterials and adipose-derived mesenchymal stem cells for regenerative medicine: a systematic review. Materials. 2021;14(16):4641. doi: 10.3390/ma14164641

[28] Torres-Guzman RA, Huayllani MT, Avila FR, et al. Application of human adipose-derived stem cells for bone regeneration of the skull in humans. J Craniofac Surg. 2022;33(1):360–363. doi: 10.1097/SCS.0000000000008114

[29] Hollinger JO, Kleinschmidt JC. The critical size defect as an experimental model to test bone repair materials. J Craniofac Surg. 1990;1(1):60–68. doi: 10.1097/00001665-199001000-00011

[30] Meek S, Mashimo T, Burdon T. From engineering to editing the rat genome. Mamm Genome. 2017;28(7–-8):302–314. doi: 10.1007/s00335-017-9705-8

[31] Jin Y, Zhang W, Liu Y, et al. rhPDGF-BB via ERK Pathway Osteogenesis and adipogenesis balancing in ADSCs for critical-sized calvarial defect repair. Tissue Eng Part A. 2014;20(23–24):3303–3313. doi: 10.1089/ten.tea.2013.0556

[32] Lough DM, Chambers C, Germann G, et al. Regulation of ADSC osteoinductive potential using notch pathway inhibition and gene rescue: a potential on/off switch for clinical applications in bone formation and reconstructive efforts. Plast Reconstr Surg. 2016;138(4):642e–652e. doi: 10.1097/PRS.0000000000002551

[33] Li S, Hu C, Li J, et al. Effect of miR-26a-5p on the Wnt/Ca2+ pathway and osteogenic differentiation of mouse adipose-derived mesenchymal stem cells. Calcif Tissue Int. 2016;99:174–186.

[34] Caetano-Lopes J, Canhao H, Fonseca JE. Osteoblasts and bone formation. Acta Reumatol Port. 2007;32:103–110.

[35] Fan J, Im CS, Guo M, et al. Enhanced osteogenesis of adipose-derived stem cells by regulating bone morphogenetic protein signaling antagonists and agonists. Stem Cells Transl Med. 2016;5(4):539–551. doi: 10.5966/sctm.2015-0249

[36] Garg P, Mazur MM, Buck AC, et al. Prospective review of mesenchymal stem cells differentiation into osteoblasts. Orthop Surg. 2017;9(1):13–19. doi: 10.1111/os.12304

[37] Lee K-S, Hong S-H, Bae S-C. Both the smad and p38 MAPK pathways play a crucial role in Runx2 expression following induction by transforming growth factor-β and bone morphogenetic protein. Oncogene. 2002;21(47):7156–7163. doi: 10.1038/sj.onc.1205937

[38] Franceschi RT, Xiao G. Regulation of the osteoblast-specific transcription factor, Runx2: responsiveness to multiple signal transduction pathways. J Cell Biochem. 2003;88(3):446–454. doi: 10.1002/jcb.10369

[39] Afzal F, Pratap J, Ito K, et al. Smad function and intranuclear targeting share a Runx2 motif required for osteogenic lineage induction and BMP2 responsive transcription. J Cell Physiol. 2005;204(1):63–72. doi: 10.1002/jcp.20258

[40] Komori T. Regulation of bone development and extracellular matrix protein genes by RUNX2. Cell Tissue Res. 2010;339(1):189–195. doi: 10.1007/s00441-009-0832-8

[41] Roca H, Phimphilai M, Gopalakrishnan R, et al. Cooperative interactions between RUNX2 and homeodomain protein-binding sites are critical for the osteoblast-specific expression of the bone sialoprotein gene *. J Biol Chem. 2005;280(35):30845–30855. doi: 10.1074/jbc.M503942200

[42] Paredes R, Arriagada G, Cruzat F, et al. Bone-specific transcription Factor Runx2 interacts with the 1α,25-dihydroxyvitamin D $_3$ receptor to up-regulate rat osteocalcin gene expression in osteoblastic cells. Mol Cell Biol. 2004;24(20):8847–8861. doi: 10.1128/MCB.24.20.8847-8861.2004

[43] Boyce BF, Xing L. Functions of RANKL/RANK/OPG in bone modeling and remodeling. Arch Biochem Biophys. 2008;473(2):139–146. doi: 10.1016/j.abb.2008.03.018

[44] Pérez-Sayáns M, Somoza-Martín JM, Barros-Angueira F, et al. RANK/RANKL/OPG role in distraction osteogenesis. Oral Surg Oral Med Oral Pathol Oral Radiol Endo. 2010;109(5):679–686. doi: 10.1016/j.tripleo.2009.10.042

[45] Gurban CV, Mederle O. The OPG/RANKL system and zinc ions are promoters of bone remodeling by osteoblast proliferation in postmenopausal osteoporosis. Rom J Morphol Embryol. 2011;52(3 Suppl):1113–1119.

[46] H'ng CH, Camp E, Anderson PJ, et al. CMTM8 is a suppressor of human mesenchymal stem cell osteogenic differentiation and promoter of proliferation via EGFR signaling. Stem Cells Dev. 2020;29(13):823–834. doi: 10.1089/scd.2020.0007

[47] He Y, Zou L. Notch-1 inhibition reduces proliferation and promotes osteogenic differentiation of bone

marrow mesenchymal stem cells. Exp Ther Med. 2019;18:1884–1890. doi: 10.3892/etm.2019.7765

[48] Hata M, Naruse K, Ozawa S, et al. Mechanical stretch increases the proliferation while inhibiting the osteogenic differentiation in dental pulp stem cells. Tissue Eng Part A. 2013;19(5–6):625–633. doi: 10.1089/ten.tea.2012.0099

[49] Moioli EK, Hong L, Mao JJ. Inhibition of osteogenic differentiation of human mesenchymal stem cells. Wound Repair Regen. 2007;15(3):413–421. doi: 10.1111/j.1524-475X.2007.00244.x

[50] Divvela SSK, Offei EB, Suerland F, et al. Atonal homolog 8/Math6 regulates differentiation and maintenance of skeletal muscle. Front Cell Dev Biol. 2022;10:950414. doi: 10.3389/fcell.2022.950414

[51] Xu N, Lao Y, Zhang Y, et al. Akt: a double-edged sword in cell proliferation and genome stability. J Oncol. 2012;2012:1–15. doi: 10.1155/2012/951724